Assessing Trajectories and Bike Handling Abilities in Road Cycling with Global Positioning System

Preprint · December 2022

DOI: 10.47953/SAE-PP-00316

1 author:

Andrea Zignoli
Università degli Studi di Trento
55 PUBLICATIONS **343** CITATIONS

SEE PROFILE

Assessing trajectories and bike handling abilities in road cycling with global positioning system data

Andrea **Zignoli**[1,†]

[1]Department of Industrial Engineering, University of Trento, Trento, Italy

[†]Corresponding author:
Mail to: Via Sommarive 9, 38123, Povo, Trento, Italy
Email: andrea.zignoli@unitn.it

Abstract

In road cycling, developing bike handling skills can prevent crashes and falling events. Nevertheless, bike handling remains largely unexplored in the world of road cycling. The goal of this research was to develop a methodology to assess bike handling during races and training, by estimating the rider-bicycle roll angle and road-plane accelerations from global positioning system (GPS) data only. A multi-dimensional bike-rider mathematical model was included into an optimal control framework to follow a reference trajectory generated from GPS data points. Estimated variables and experimental data collected with a cost effective setup showed good agreement: i.e., root mean square error (RMSE) of 12° and 0.1 g for roll angle and both longitudinal and lateral accelerations respectively, in the worst-case scenarios. This methodology might allow for the estimation of key bike handling variables during fast segments with cost effective instrumentation. It can therefore constitute a tool for objectively assessing bike handling in road cycling training and racing.

Keywords: bike-rider model; optimal control; cycling computers;

1. INTRODUCTION

While experiencing an increase in the number of crashes, the world of road cycling races is calling for measures that can improve riders' safety conditions (1). Developing a rider's technical skillset is an essential component of safe and optimal performances.

The forces that the riders can generate while riding a bike are generated at the tyre-road interface (i.e., the contact patch). Contact forces can act both in the longitudinal and the lateral directions i.e., tangentially, and orthogonally to the bike-rider system velocity. Longitudinal forces can be responsible for relevant accelerations during propulsive and braking actions. Lateral forces cause the lateral accelerations while riders are following curved paths. When riders use the handlebars and their body weight to steer and lean inside the corners, the magnitude of the lateral forces are largely determined by the angular displacement of the bike-rider system about the longitudinal axis (i.e., the roll angle).

The tyre-road interaction can only provide a maximum amount of grip force and, if the limit is exceeded suddenly or unexpectedly, the rider might lose control of the bike. A direct estimation of the magnitude of these forces can be obtained with the product of the vertical load acting on the tyre and the friction coefficient between the tyre and road surfaces. An indirect estimation of these forces can be provided by the longitudinal and lateral accelerations of the bike-rider system.

In the world of practice, bike handling refers to the performance of the rider-bike interaction, and much of the scientific research has been devoted to the design of guidelines to improve bicycle stability and manoeuvrability (2). Bike handling remains, however, largely unexplored in road cycling races, especially from a sport performance perspective. Test batteries are the most common tools for objectively differentiating riders with good and bad bike handling. It is very difficult for coaches to go beyond the results of the battery tests and provide the riders with indications about how to improve their bike handling and gain a competitive advantage.

Retrieving data that can be used to assess bike handling performance during road cycling races or training is highly problematic. In the world of both amateur and professional races, bikes are typically only instrumented with lightweight/compact cycling computers. These devices are equipped with the global positioning system (GPS) receivers, and they are used to derive important information about cycling performance, such as total elevation gain and average speed. Cycling computers are usually not equipped with inertial measurement units (IMU), and they receive and fuse together information derived from both the GPS and an odometer positioned at the front wheel to get a reliable estimation of the travelling distance and speed in case of obstructions, e.g.: tunnels, trees, buildings, clouds, etc. Cycling computers are often equipped with a barometer or/and a mono-axial inclinometer which provides an estimation of the slope of the road. Given the absence of an onboard embedded IMU, information about the orientation of the bicycle is limited to the pitch (i.e., the angular displacement of the bike-rider system about its transversal axis) provided by the inclinometer (when present), and information about the roll angle and the lateral accelerations are usually not available.

Information about the longitudinal a_x and lateral a_y bicycle accelerations are particularly useful for bike handling assessment. For example, the g-g-diagram (3) consists in a graph where the lateral acceleration values are plotted against the longitudinal acceleration values. The limits of the friction forces are provided by the friction ellipse defined as follows:

$$\left(\frac{a_x(s)}{\mu_x\, g}\right)^2 + \left(\frac{a_y(s)}{\mu_y\, g}\right)^2 \leq 1, \qquad (1)$$

where μ_x and μ_y are the tyre-road friction coefficients in the longitudinal and lateral directions and g is the magnitude of acceleration due to gravity. Possible differences between μ_x and μ_y are due to the shape of the tyre-road contact patch, and they heavily depend on tyre shape and conformation (see e.g. (4)). The shape of the distribution of the acceleration values inside the friction ellipse can be used to evaluate different riding styles, e.g.: the combination of the acceleration values lying inside the adherence ellipse are considered safe. It is reasonable to think that the riders who can consciously and consistently ride close to the limits imposed by the friction ellipse without losing control of their bikes, are the ones with better bike handling.

Several methods to estimate the longitudinal, lateral accelerations and the roll angle on two-wheeled vehicles with inexpensive hardware have been developed. For example, Boniolo et. al (6) and Lot et al. (7) developed a methodology to estimate the roll angle from gyroscopes and encoders on motorcycles. Gasbarro et al. (8) developed an algorithm for the reconstruction of the trajectory of a motorcycle starting from an onboard camera and accelerometers. Schlipsing et al. (9) developed a method to estimate the roll angle in motorcycles from grayscale images collected with an onboard camera. More recently, a cost effective method to estimate the roll angle from a gyroscope on city bicycles has been proposed by Sanjurjo et al.

(10). In 2016, Cain (11) presented a new methodology where 11 wireless IMUs were used to sense the separated movements of the bicycle and rider. A Kalman filter was used by Cain to estimate the orientation of the bike-rider system. The method proposed by Sanjurjo et al. (10) requires a Kalman filter to be developed for the estimation of the bias in the roll angle measurements. Sanjurjo et al. (10) reported that their method (conceived for city bicycles) can provide a roll angle estimation with less than 2° of error. For the method proposed by Lot et al. (7) for motorcycles, authors reported an error in the estimation of 4° (7). Both Baniolo et al. (6), Lot et al. (7) and Sanjurjo et al. (10) adopted distance sensors to collect the gold-standard roll angle of the vehicle.

Although the aforementioned methodologies differ in hardware configuration and data processing procedure, they all make use of a mathematical model of the bike-rider system dynamics. In these models, there is always a set of variables (i.e., the state variables) that can be used to describe the mathematical state of the system and to determine its future behaviour. To study bike handling, the roll angle and the lateral and longitudinal accelerations (or their mathematical primitives) should be included in the set of state variables. If some of the state variables can be directly measured (e.g., position on the road plane from GPS), then experimental data can be incorporated into the model to estimate the unknown variables (e.g., roll angle, longitudinal and lateral accelerations) (12). This process of estimating the unknown variables consists of finding the set of input variables (e.g., the steering angle or the power output), so the difference between the simulated and experimental data is minimised. The solution is often provided with dynamic optimisation techniques such as optimal control (13).

The goal of this research was to establish a methodology to estimate roll angle and longitudinal and lateral accelerations in road cycling using GPS data. A model of bike-rider system dynamics developed in a previous research (13) was used here in an optimal control framework. The values of the variables estimated with the model have been compared against experimental data collected on the field with a cost effective experimental setup (mobile phone equipped with IMU).

2. METHODS

A multi-dimensional model of bike-rider dynamics (13) was used in this study. An optimal control solver (16) was used to track the reference trajectory. The reference trajectory was computed by fitting the GPS data. Variables estimated with the model (roll angle and longitudinal and lateral accelerations) were compared to experimental data collected with a mobile phone equipped with IMU. In this section, all the different elements of the analysis are discussed in details.

2.1 The rider-bicycle model: The bike-rider system has been modelled as an inverted pendulum with a single-mass point moving on a plane (i.e., *xy*) along a curve (**Fig. 1**) and tilting with a roll angle φ. Two inputs were used to control the system: the normalized steering angle δ_n (between maximal and minimal values δ_{min} and δ_{max}) and power output W_n (between W_{min} and W_{max}).

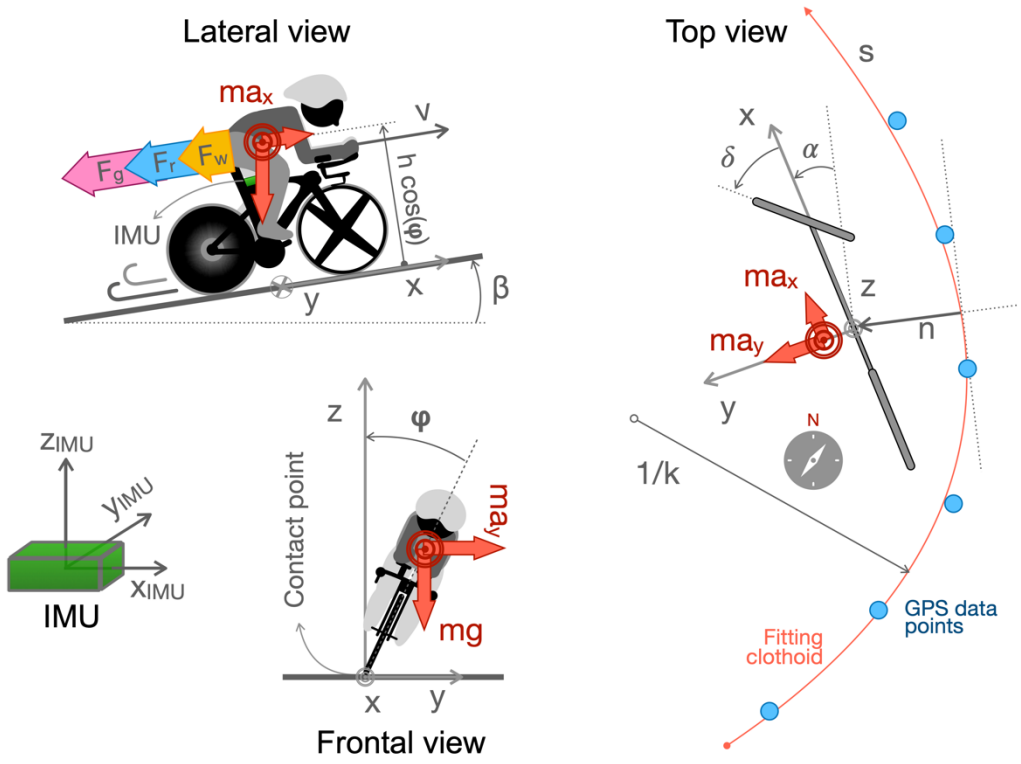

Fig. 1 Schematic representation of the rider-bicycle model. The three axes x, y and z are pointing forward, leftward and upward, respectively. This holds also for the three axes of the inertial measurement unit IMU: x_{IMU}, y_{IMU} and z_{IMU}. **Lateral view**: resistance aerodynamic F_w, rolling F_r and gravitational F_g forces are reported. Longitudinal acceleration a_x and the action of gravity are reported. The height of the centre of mass is h and the slope of the road β are reported. The position of the IMU is highlighted. **Frontal view**: longitudinal acceleration a_x, the action of gravity and roll angle φ are reported. **Top view**: a generic clothoid (Euler spiral) fitting global positioning system (GPS) points was used as reference trajectory. The distance from the start of the clothoid is the curvilinear abscissa s and the lateral distance from the clothoid *is* n. Vehicle heading α, steering angle δ, the action of the longitudinal a_x and lateral a_y accelerations, the curvature radius $1/k$ of the reference trajectory are reported. The schematic compass indicates the true North.

The forces created at the tyre-road interfaces are applied to a single point of contact, i.e.: the lower extremity of the pendulum at z=0. The mass of the rider and the bicycle were set to 76 kg and 9 kg, respectively. In cycling, resistive forces have three main components (17): 1) aerodynamic forces F_w (18) were computed as the half of the product of the air drag force coefficient k_v (0.15 *kg/m*, i.e. the product of a drag coefficient C_D of 0.7, a frontal area A_f of 0.35 m^2 and an air density ρ of 1.23 kg/m^3 (19)) and the squared longitudinal speed v; 2) the rolling resistive forces F_r (20) were computed as the product of the rolling coefficient C_{rr} (0.004 (21)) and the mass of the system, the cosine of the road slope β and the constant of gravity g; 3) the gravitational force F_g was computed as the product of the mass of the system m, the sine of the road slope β and the magnitude of acceleration due to gravity. Clothoids (i.e., Euler spirals) were used to fit the GPS data points and to define the reference trajectory of the rider-bicycle model. Clothoids are commonly used to describe curvilinear trajectories because their curvature k changes linearly with the curve length. This is extremely important because a linear change in the curvature allows for the definition of smooth transitions between paths, without abrupt changes in centripetal acceleration values. Curvilinear coordinates (22) were used to define the position of the bicycle: s constitutes therefore the longitudinal position, n is the

lateral displacement of the centre of mass, α is the heading and $1/k$ is the local radius of the single clothoid segment (**Top view, Fig. 1**).

2.2 The system of equations: With the introduction of the curvilinear coordinates, the curvilinear abscissa was used as independent variable instead of the time *t*. The equations of motions were obtained for the bike-rider system, and differential equations were solved in their explicit form to highlight the variations of the state variables with respect to *s*. The following substitution law was used:

$$\frac{d}{ds}\dot{s}(s) = \frac{d}{ds}\frac{ds}{dt}, \tag{2}$$

where the classic notation $\dot{x}$ indicates the time derivative of a generic variable *x*. This was done to improve the readability of the equations. The first equation of the dynamics defines the variation of α with *s*:

$$\frac{d}{ds}\alpha(s) = \frac{\delta_n(s)\delta_{max}}{L\,\dot{s}(s)} - k(s), \tag{3}$$

where L is the wheelbase of the bike. The second equation of the dynamics defines the variation of *n* with *s*:

$$\frac{d}{ds}n(s) = \frac{1}{\dot{s}(s)}(v(s)\sin(\alpha(s))) \tag{4}$$

The third equation of the dynamics defines the variation of *v* with *s*:

$$\frac{m\,v(s)}{W_{max}}\frac{d}{ds}v(s) = \frac{W_n(s)}{\dot{s}(s)} - \frac{v(s)}{\dot{s}(s)W_{max}}\left(m\,g\left[C_{rr}\cos(\beta(s)) + \sin(\beta(s))\right] + k_v(v(s) - V_w(\alpha(s))^2\right), \tag{5}$$

where V_W is the wind velocity (which is dependent on the heading). The fourth equation of the dynamics defines the variation of φ with *s*:

$$\frac{d}{ds}\varphi(s) = \frac{\dot{\varphi}(s)}{\dot{s}(s)} \tag{6}$$

The fifth equation defines the variation of the time derivative of φ with *s*:

$$\frac{d}{ds}\dot{\varphi}(s) = \frac{h\,m\,g}{I_X g\,L\,\dot{s}(s)}(v(s)^2\delta_{max}\delta_n(s) + L\,g\,\varphi(s)), \tag{7}$$

where *h* is the distance between the contact point on the road plane and the position of the centre of mass of the bike-rider system and I_X is the moment of inertia of the system along the longitudinal direction. The sixth equation defines the variation of W_n with *s*:

$$\frac{d}{ds}W_n(s) = \frac{\dot{W}_n(s)}{\dot{s}(s)} \tag{8}$$

The seventh equation defines the variation of δ_n with *s*:

$$\frac{d}{ds}\delta_n(s) = \frac{\dot{\delta}_n(s)}{\dot{s}(s)} \tag{9}$$

The eighth equation defines the variation of the time derivative of *s* with *s*:

$$\frac{d}{ds}\dot{s}(s) = \frac{v(s)\cos(\alpha(s))}{1 - n(s)k(s)} \tag{10}$$

The ninth equation defines the variation of *t* with s:

$$\frac{d}{ds}t(s) = -\frac{1 + k(s)n(s)}{cos(\alpha(s))v(s)} \tag{11}$$

2.3 Optimal control problem formulation: The main building blocks of an optimal control problem are: the system of equations (eqns. 2-11 presented in the previous subsection), the objective function, the initial conditions, and the constraints.

The optimal control was used to find the combination of inputs that could minimize the objective function *J*. The objective function was defined as the weighted sum of three different goals:

$$J = J_1 + J_2 + J_3 \tag{12}$$

The first two terms (J_1 and J_2) included the discrepancies between experimental and simulated data (lateral displacement *n* from the fitting clothoid and longitudinal speed *v*):

$$J_1 = \int_{L_0}^{L_f} \frac{(v(t) - v^*(t))^2}{\Delta w_v{}^2} \frac{1}{\dot{s}(s)} ds \tag{13}$$

$$J_2 = \int_{L_0}^{L_f} \frac{(n(t))^2}{\Delta w_n{}^2} \frac{1}{\dot{s}(s)} ds \tag{14}$$

The third term (J_3) included the rate of change of the steering angle $\dot{\delta}$ and the rate of change of the power output $\dot{W}$ (13):

$$J_3 = \int_{L_0}^{L_f} \frac{1}{\dot{s}(s)} \left(1 + \left(\frac{v_\delta}{\Delta w_\delta^2 \dot{\delta}_{max}}\right)^2 + \left(\frac{v_W}{\Delta w_W^2 \dot{W}_{max}}\right)^2\right) ds \tag{15}$$

Each of these three terms was weighted differently with a coefficient (i.e.: $1/\Delta w_v$, $1/\Delta w_n$, $1/\Delta w_\delta$ and $1/\Delta w_W$, for the longitudinal speed *v*, the lateral displacement *n*, the rate of change of the steering angle $\dot{\delta}$ and the rate of change of the power output $\dot{W}$) in the cost function.

Some constraints were imposed to the optimal control problem. The steering angle δ and the power output *W* were constrained between their maximal and minimal values (i.e.: δ_{max}, δ_{min}, W_{max} and W_{min}). The resulting constraints therefore were:

$$-1 \leq \delta_n(s) \leq 1 \tag{16}$$

$$-1 \leq W_n(s) \leq 1 \quad (17)$$

The maximal power output was reduced to *zero* for roll angles greater than 15° (this is because cyclists usually do not pedal while cornering).

Initial values for all the state variables were set to zero, except for the longitudinal velocity which was set with the initial velocity provided by the GPS. The software Maple (Maplesoft, ver. 2018) and MBSymba (23) toolbox were used to formulate and manipulate the equations of the dynamic system. The XOptima toolbox and the software PINS (16) were used to formulate and then solve the optimal control problem. The distance between the nodes of the mesh of the optimal control problem was set to 0.5 m.

2.4 The courses: The courses selected for the data collection were characterized by:

- *Course 1:* was characterized by total length of 5.8 km, a total elevation loss of 263 m, three fast S-turns, one hair-pin turn with decreasing radius, two 90-deg turns, one fast long turn, a longer flat segment and a final round-about.
  The course profile and map can be found at:
  https://www.google.com/maps/d/u/1/edit?mid=1yeyWb-_jFGclNPZM-kwn3Fhiv2wWfq9F&usp=sharing

- *Course 2:* was characterized by total length of 5 km, a total elevation loss of 288 m, three fast S-turns, eight hair-pin turns, two 90-deg turns, one fast long turn. The course profile and map can be found at:
  https://www.google.com/maps/d/u/1/edit?mid=19sOCsULkUimzP-Xkp9uNyr-lITbSMZfj&usp=sharing

An amateur cyclist (i.e., average distance cycled in the last 5 years: 2500 km/year), was asked to complete the courses on separate days. Asphalt was dry and similar temperature and humidity and non-windy conditions were checked before each course. Because there was no cycling lane, the cyclist was asked to keep to the right lane to avoid dangerous collisions with incoming vehicles. The cyclist knew the courses in advance and was asked to complete the course at a self-selected speed.

2.5 Experimental data collection: A road bicycle with aerobars was equipped with a Smartphone (Xiaomi Mi 10 lite), able to collect synchronized data from the embedded accelerometer (Bosch BMA 490L, 200 *Hz*), the gyroscope (Bosch BMG 250, 500 *Hz*) and the dual frequency GPS receiver (L1/L5 frequencies). A custom written Matlab (Mathworks, ver. 2020a) was used to process the GPS data points and compute the parameters of the trajectory clothoids. The Smartphone was fixed to the bicycle frame horizontally on the top tube at the junction with the seat tube. This position was selected because it was near enough to the actual centre of mass of the actual system. The three axes of the inertial measurement unit (IMU) (i.e.: x_{IMU}, y_{IMU} and z_{IMU}, **Fig. 1**) were pointing forward, leftward and upward. The accelerometer provided three accelerations along the three axes of the IMU: a^*_{xIMU}, a^*_{yIMU} and a^*_{zIMU}. The accelerometer also acted as inclinometer to provide the experimental pitch ϑ^* (i.e., proxy for the angular displacement of the bike-rider system about its transverse axis), roll φ^* (i.e., proxy for the roll angle: the angular displacement of the bike-rider system about its longitudinal axis) and yaw ψ^* (i.e., proxy for the yaw angle: the angular displacement of the bike-rider system about its normal axis). The gyroscope provided three angular rates along the three axes of the

IMU: ω^*_{xIMU}, ω^*_{yIMU} and ω^*_{zIMU}. The Physics Toolbox Sensor suite application (24) for Android was used to log and then export the experimental data. The data from the IMU were logged with a non-constant sampling time of 0.0092±0.01 s. It has been noticed that the GPS data were logged with slower frequency of 1±0.01 s and with an average delay of 0.9 s with respect to the data from the IMU. This delay has been considered and signals have been correctly aligned. GPS data points were written in a *kml* file and they were used to estimate the road slope β by means of the GPS-visualizer on-line tool (gpsvisualizer.com). Experimental longitudinal speed v^* was also computed from GPS data.

One big issue with measuring/estimating the roll angle with an accelerometer is that it can be used to estimate the roll angle only during steady-state cornering, i.e.: a condition where a trajectory with constant radius is negotiated at constant speed and constant yaw rate. The method proposed by Boniolo et al. (6) was used here to get closer to the actual conditions:

$$\varphi_b^* = \varphi_{LF}^* + \varphi_{HF}^* \tag{9}$$

Where φ^*_{LF} and φ^*_{HF} are the low- and high-frequency (smaller and larger of 0.15 Hz, respectively) components of the experimental roll angle φ^*. The φ^*_{HF} is computed by simple numerical integration of the high frequency component of the experimental angular rate $\omega^*_{xIMU\text{-}HF}$. The φ^*_{LF} is computed by means of the low-frequency components of the experimental longitudinal speed v^*_{LF} and $\omega^*_{zIMU\text{-}LF}$ (6).

Experimental longitudinal and lateral accelerations on the road plane were computed as the projections of the accelerations provided by the IMU on the *xy* plane (**Fig. 1**).

Differences between the values provided by the model and the IMU experimental data were computed for the roll angle and the longitudinal and lateral accelerations. The root mean square error (RMSE) was used to express the magnitude of these differences.

3. RESULTS

Across the different segments of the courses, the cyclist mainly adopted 4 different positions, which qualitatively presented in **Fig. 2**.

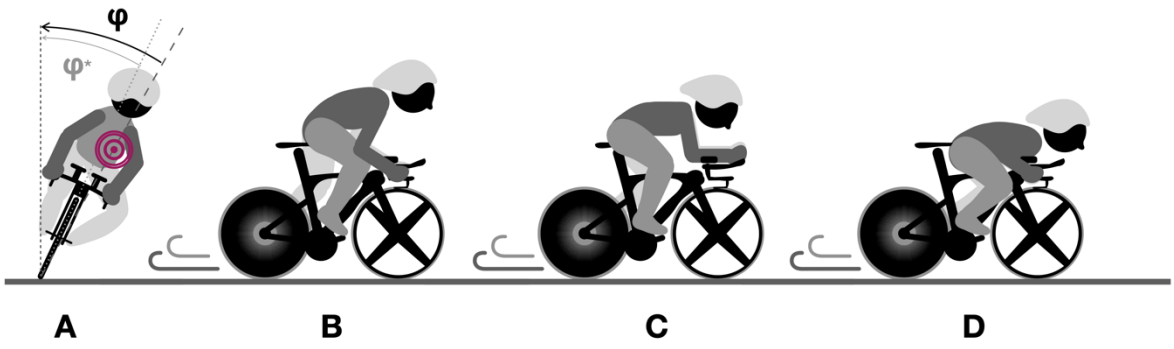

Fig. 2 Schematic representation of the most common cycling positions adopted by the cyclist in this study. **A**) Cornering position where the roll angle of the actual rider-bicycle system φ and the roll angle φ^* measured by the inertial measurement unit (IMU) are reported. **B**) Standing position. **C**) Aero position. **D**) Descending position.

Course 1: In total, 151 clothoids were used to fit the GPS experimental data points. The average difference between the fitting clothoids and the experimental points was 0.05±0.049 m, and the maximal error was 0.65 m. The course was completed in 8'39" with an average speed of 42.2 km/h. On the entire course, an RMSE of 6.5° has been computed for the roll angle estimation, and the RMSE values for the longitudinal and lateral accelerations were 0.06 g and 0.07 g respectively. Across the 200 m including the round-about, the RMSE changed to 9.5°, 0.05 g and 0.1 g for the roll angle, longitudinal and the lateral accelerations, respectively. Across the 200 m including the fast 90-deg turn, the RMSE was 8.2°, 0.07 g and 0.1 g for the roll angle, longitudinal and the lateral accelerations, respectively. Example of the comparisons between simulated and experimental data on the entire course are reported in **Fig. 3**.

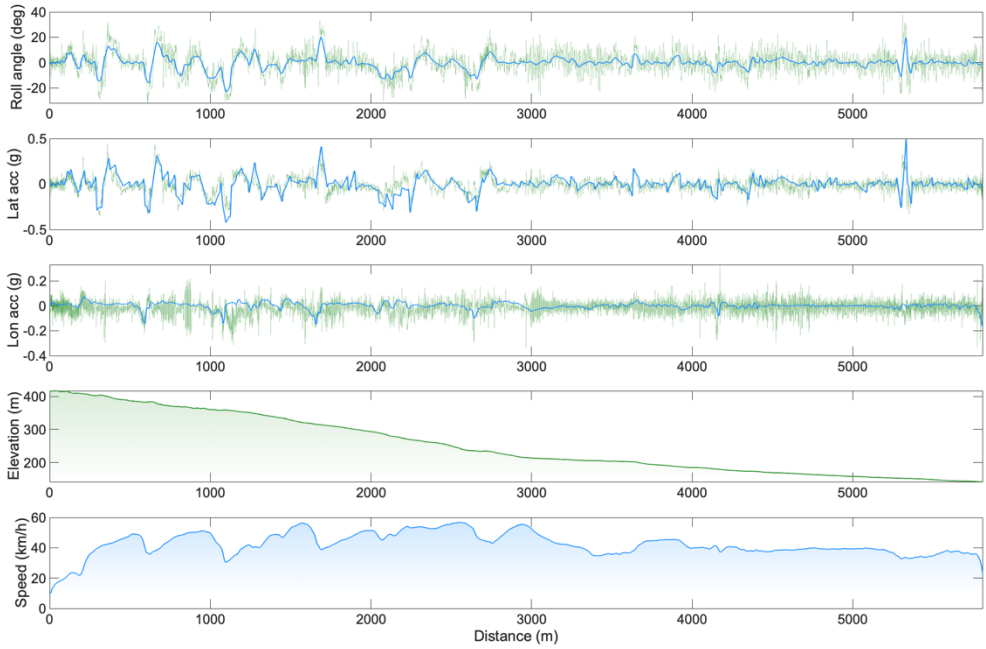

Fig. 3 Comparison between simulated (blue) and experimental data (light green) for the first course. From top to bottom: roll angle, lateral acceleration, longitudinal acceleration, elevation and speed.

Course 2: In total, 130 clothoids were used to fit the GPS experimental data points. The average difference between the fitting clothoids and the experimental points was 0.12±0.13 m, and the maximal error was 1.1 m. The course was completed in 7'36" with an average speed of 41.5 km/h. On the entire course, an RMSE of 8.7° has been computed for the roll angle estimation, and the RMSE values for the longitudinal and lateral accelerations were 0.1 g and 0.13 g respectively. Across the 200 m including one of the hair-pin turns, the RMSE changed to 12.3°, 0.12 g and 0.17 g for the roll angle, longitudinal and the lateral accelerations, respectively. Examples of the comparisons between simulated and experimental data on the entire course are reported in **Fig. 4**.

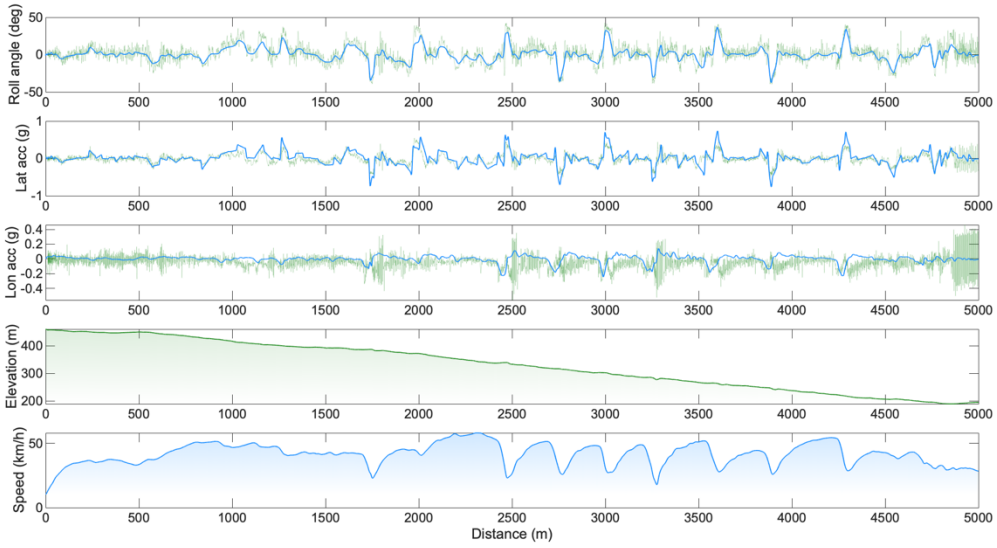

Fig. 4 Comparison between simulated (blue) and experimental data (light green) for the second course. From top to bottom: roll angle, lateral acceleration, longitudinal acceleration, elevation and speed. In the very last portion of the signal, a strong pedalling action generating sharp lateral accelerations can be noticed.

4. DISCUSSION

The methodology presented in this paper has been conceived for road cycling races and for fast descending sections. Data collected on two different courses, that could constitute typical segments in road cycling races, was used to assess the accuracy of the estimations in roll angle, longitudinal and lateral accelerations. Provided that only GPS data were used in this research, an RMSE range of 6.5-12.3° in the estimation of the roll angle constitutes an encouraging result, but improvements are possible. In comparison with the errors reported by Baniolo et al. (6) (5° in the roll angle estimation) the error is almost double, but still deemed acceptable. Boniolo et al. (6), in their experimental work declared an additional error of 2° due to the tyre-cross section of their vehicle (i.e., a motorcycle). It can be assumed that, in bicycles, the tyre-cross section introduces a negligible error due to the tyre-cross sectional area (for a bicycle the contact point can be assumed to lie on the bicycle symmetry plane (7)).

In the present work, the IMU was fixed to the frame of the bike. Another option would have been to fix the IMU to the body of the cyclist. Placing the IMU on the frame of the bike can provide abrupt lateral accelerations because the cyclist's pedalling action. During actual cycling races, cycling computers are placed on the handlebars. This is because riders can benefit from visual feedback by checking the display of the computer. Even if cycling computers were equipped with an IMU, estimating the roll angle with an IMU fixed on the handlebars would be challenging. This is because there would be an additionally complex influence of the steering angle. In light of these considerations, the ranges of the RMSE reported for the longitudinal (0.05-0.12 g) and the lateral (0.1-0.17 g) accelerations can be considered an encouraging result. In a recent paper, Zignoli et al. (25) showed that magnitude of accelerations is associated with performance in downhill sections in road cycling. Inter-individual difference between cyclists might be compatible with the error reported here. Evaluating whether this methodology can be used to assess the difference between experts and novice riders, or to classify riders by bike-handling ability was deemed out of scope. This might become the subject of a next research work.

Graphs reported in **Fig. 3** and **Fig. 4** can be used to spot the sections of the course where the error in the estimation was maximum. Most of the errors in the estimation could be due to the changes in the riding position. In these regards, fixing the IMU on the body of the cyclist would include different information due to the cyclist's body displacement (11). The most problematic positions were the first and second riding positions (**A** and **B**, **Fig. 2**). The first was the cornering position: the cyclist needed to move the hands from the aerobars to the hoods to improve bicycle manoeuvrability. In this position, is likely that the upper body motion could move the centre of mass of the system away from the plane of symmetry of the vehicle, where the IMU was positioned (i.e., discrepancy between measured roll angle φ^* and actual roll angle of the rider-bicycle system φ). Another problematic position is reported in B, **Fig. 2**. This standing position was used by the cyclist to deliver high torque values and accelerate after the corners. In this position, IMU likely sensed strong accelerations due to the pedalling action (these strong accelerations can be easily spotted in **Fig. 4**, towards the end of the course).

The greater RMSE values reported for the small segments (i.e., hairpin turns or round about, clearly discernible in **Fig. 3** and **Fig. 4**) reinforce the idea that the estimation of the roll angle and the road-plane accelerations might be problematic in slow segments, where cyclists are asked to brake, turn frequently and re-accelerate. Two other common riding positions are reported in C and D, **Fig. 2**. In these positions, the centre of mass of the system was better aligned with the plane of symmetry of the vehicle. In the aero C position, the cyclist was pedalling with a steady action and the arms were placed on the handlebars. In the descending D position, the cyclist was not pedalling, the chest was placed on the handlebars and the hands were placed on the hoods. This methodology is expected to be particularly accurate and reliable on fast road segments (where riding positions C and D are commonly adopted), where additional complexities not considered in the rider-bicycle dynamic model could only play a marginal role.

Another potential limitation is that the road geometry has been considered flat, without any banking. The information about this angle is particularly complex to retrieve, especially in long road segments. Unfortunately, no information is available on the amount of banking of the two courses. This adds more uncertainty to the estimation of the roll angle, which is affected by the road banking angle. The model developed by Fitton and Symons for track cycling (26), for instance, takes the banking angle into consideration, but it has been developed mainly for track cycling, where racing sections are considerably shorter than in road cycling.

The accuracy of this methodology might not be sufficient to provide a reliable source of information for the design of safety action controllers. Safety controllers usually operate in high-stakes environments, and they need accurate and reliable information about the state of the bike-rider system. However, the accuracy of the present methodology might be sufficient to develop indexes for the different standard manoeuvres and classify good and bad handling in cyclists, e.g., by examination of the adherence ellipse, as it was done in (25). It is worth highlighting that this methodology only relies on GPS data and therefore can be easily accessed by a large pool of practitioners. In the world of sports sciences, quantitative handling research in road cycling races is very limited. The use of this methodology in the development of a set of guidelines for different levels of bike-handling ability could help manufacturers designing racing bicycles that are conceived for specific groups, such as: 'rookie', 'transitional' or 'daredevil'. Coaches and athletes could use this tool to run data analyses in post process and test/develop specific training for technical skills development.

5. CONCLUSIONS

With the goal of developing a standard cost effective tool for assessing bike handling skills in road cycling training and races, a rider-bicycle model was deployed in an optimal control framework to estimate roll angle, longitudinal and lateral accelerations from GPS data on road bicycles. The accuracy of the roll angle estimations slightly exceeds that reported for other similar methods exploiting other cost effective hardware solutions (e.g., onboard gyroscopes or accelerometers). Importantly, the methodology presented in this paper only relies on GPS data and therefore can motivate a step forward in the deployment of this methodology on cycling computers. This would allow a rapid spread of more in-depth bike handling performance indexes in road cycling.

Ethic statement

Ethics approvals for this study has been received from the Ethic Committee of the University of Trento (approval number 2021-010). This research has been conducted in agreement with the Declaration of Helsinki for the research involving human subjects. An informed consent was signed by the participant of this study before taking part to the experimental data collection.

Funding details

No funding was received for the present work.

Disclosure statement

No potential competing interest was reported by the authors.

Data availability statement

Data associated to this manuscript will be open and fully available and will be deposited in a recognized data repository upon acceptance.

Appendix

A.1 Numerical values and list of symbols

$a_{xmax} = a_{ymax} = 9.81$ m/s^2, longitudinal and lateral maximal accelerations
$g = 9.81$ m/s^2, constant of gravity
$h = 1$ m, height of the centre of mass from road surface
$k_v = ½\ A_f\ C_D\ \rho = 0.15$ kg/m, air drag force coefficient
$m = 85$ kg, cyclist's body mass + bicycle mass
$n_0 = 0$ m, initial lateral displacement
$s_0 = L_0 = 0$ m, initial longitudinal position
$\dot{W}_{max} = 50$ W/s, maximal rate of power output
$w_D = \pi$ rad, wind direction

$A_f = 0.35$ m^2, frontal area
$C_D = 0.7$, drag coefficient
$C_{rr} = 0.004$, rolling friction coefficient

I_X = 77 kgm^2, inertia of the system along the longitudinal direction
L = 1.4 m, wheelbase
L_f = m, course length
V_w = 0 m/s, wind speed
W_{n0} = 0, initial normalised power output
W_{max} = 1200 W, maximal power output

α_0 = 0 rad, initial heading
Δw_n = 1, weight of the lateral displacement in the objective function
Δw_v = 1, weight of the error with the reference velocity in the objective function
Δw_w = 10, weight of the rate of change of the steering angle in the objective function
Δw_δ = 10, weight of the rate of change of the power output in the objective function
δ_{max} = 0.52 rad, maximal steering angle
$\dot{\delta}_{max}$= 0.52 rad/s, maximal steering angle
δ_{n0} = 0, initial normalised steering angle
φ_0 = 0 rad, initial rolling angle
$\dot{\varphi}_0$= 0 rad/s, initial roll rotational velocity
ρ = 1.23 kg/m^3, air density

Bibliography

1. UCI - Press releases. Road cycling: the UCI announces the introduction of numerous measures to improve rider safety as of 2021 [Internet]. 2020. Available from: https://www.uci.org/inside-uci/press-releases/road-cycling-the-uci-announces-the-introduction-of-numerous-measures-to-improve-rider-safety-as-of-2021

2. Kooijman JDG, Schwab AL. A review on bicycle and motorcycle rider control with a perspective on handling qualities. Vehicle System Dynamics. 2013 Nov;51(11):1722–64.

3. Rice RS. Measuring car-driver interaction with the gg diagram. SAE Technical Paper; 1973. Report No.: 0148–7191.

4. Dressel A, Sadauckas J. Characterization and Modelling of Various Sized Mountain Bike Tires and the Effects of Tire Tread Knobs and Inflation Pressure. Applied Sciences. 2020 May 1;10(9):3156.

5. Schwab AL, Meijaard JP. A review on bicycle dynamics and rider control. Vehicle System Dynamics. 2013 Jul;51(7):1059–90.

6. Boniolo I, Tanelli M, Savaresi SM. Roll angle estimation in two-wheeled vehicles. IET Control Theory & Applications. 2009 Jan 1;3(1):20–32.

7. Lot R, Cossalter V, Massaro M. Real-Time Roll Angle Estimation for Two-Wheeled Vehicles. In: Volume 1: Advanced Computational Mechanics; Advanced Simulation-Based Engineering Sciences; Virtual and Augmented Reality; Applied Solid Mechanics and Material Processing; Dynamical Systems and Control [Internet]. Nantes, France: American Society of Mechanical Engineers; 2012 [cited 2020 Nov 14]. p. 687–93. Available from: https://asmedigitalcollection.asme.org/ESDA/proceedings/ESDA2012/44847/687/232314

8. Gasbarro L, Beghi A, Frezza R, Nori F, Spagnol C. Motorcycle trajectory reconstruction by integration of vision and MEMS accelerometers. In: 2004 43rd IEEE Conference on Decision and Control (CDC) (IEEE Cat No04CH37601) [Internet]. Nassau, Bahamas: IEEE; 2004 [cited 2020 Nov 16]. p. 779-783 Vol.1. Available from: http://ieeexplore.ieee.org/document/1428759/

9. Schlipsing M, Schepanek J, Salmen J. Video-based roll angle estimation for two-wheeled vehicles. In: 2011 IEEE Intelligent Vehicles Symposium (IV) [Internet]. Baden-Baden, Germany: IEEE; 2011 [cited 2020 Nov 16]. p. 876–81. Available from: http://ieeexplore.ieee.org/document/5940533/

10. Sanjurjo E, Naya MA, Cuadrado J, Schwab AL. Roll angle estimator based on angular rate measurements for bicycles. Vehicle System Dynamics. 2019 Nov 2;57(11):1705–19.

11. Cain S. Measurement of Bicycle and Rider Kinematics during Real-World Cycling Using a Wireless Array of Inertial Sensors. 2016;698520 Bytes.

12. Biral F, Bortoluzzi D, Cossalter V, Lio M. Experimental Study of Motorcycle Transfer Functions for Evaluating Handling. Vehicle System Dynamics. 2003 Jan 1;39(1):1–25.

13. Zignoli A, Biral F. Prediction of pacing and cornering strategies during cycling individual time trials with optimal control. Sports Eng. 2020 Dec;23(1):13.

14. Fujii S, Shiozawa S, Shinagawa A, Kishi T. Steering characteristics of motorcycles. Vehicle System Dynamics. 2012 Aug;50(8):1277–95.

15. Zignoli A. Influence of corners and road conditions on cycling individual time trial performance and 'optimal' pacing strategy: A simulation study. Proceedings of the Institution of Mechanical Engineers, Part P: Journal of Sports Engineering and Technology. 2020 Nov 30;175433712097487.

16. Biral F, Bertolazzi E, Bosetti P. Notes on Numerical Methods for Solving Optimal Control Problems. IEEJ Journal of Industry Applications. 2015;5:154–66.

17. De Groot G, Welbergen E, Clusen L, Clarus J, Cabri J, Antonis J. Power, muscular work, and external forces in cycling. Ergonomics. 1994;37(1):31–42.

18. Grappe F, Candau R, Belli A, Rouillon JD. Aerodynamic drag in field cycling with special reference to the Obree's position. Ergonomics. 1997 Dec;40(12):1299–311.

19. Crouch TN, Burton D, LaBry ZA, Blair KB. Riding against the wind: a review of competition cycling aerodynamics. Sports Eng. 2017 Jun;20(2):81–110.

20. Grappe F, Candau R, Barbier B, Hoffman MD, Belli A, Rouillon JD. Influence of tyre pressure and vertical load on coefficient of rolling resistance and simulated cycling performance. Ergonomics. 1999 Oct;42(10):1361–71.

21. Burke E. High-tech cycling. Human Kinetics; 2003.

22. Lot R, Biral F. A curvilinear abscissa approach for the lap time optimization of racing vehicles. IFAC Proceedings Volumes. 2014;47(3):7559–65.

23. Lot R, Da Lio M. A symbolic approach for automatic generation of the equations of motion of multibody systems. Multibody System Dynamics. 2004;12(2):147–72.

24. Vieyra R, Vieyra C, Jeanjacquot P, Marti A, Monteiro M. Turn your smartphone into a science laboratory. The science teacher. 2015;82(9):32.

25. Zignoli A, Biral F, Fornasiero A, Sanders D, Erp TV, Mateo-March M, et al. Assessment of bike handling during cycling individual time trials with a novel analytical technique adapted from motorcycle racing. European Journal of Sport Science. 2021 Aug 7;1–23.

26. Fitton B, Symons D. A mathematical model for simulating cycling: applied to track cycling. Sports Engineering. 2018;21(4):409–18.